

Realization of a double-slit SQUID geometry by Fermi arc surface states in a WTe₂ Weyl semimetal.

O.O. Shvetsov,¹ A. Kononov,¹ A.V. Timonina,¹ N.N. Kolesnikov,¹ and E.V. Deviatov¹

¹*Institute of Solid State Physics of the Russian Academy of Sciences,
Chernogolovka, Moscow District, 2 Academician Ossipyan str., 142432 Russia*

(Dated: January 30, 2018)

We experimentally study electron transport between two superconducting indium leads, coupled to the WTe₂ crystal surface. WTe₂ is characterized by presence of Fermi arc surface states, as a predicted type-II Weyl semimetal candidate. We demonstrate Josephson current in unprecedentedly long 5 μm In-WTe₂-In junctions, which is confirmed by $I - V$ curves evolution with temperature and magnetic field. The Josephson current is mostly carried by the topological surface states, which we demonstrate in a double-slit SQUID geometry, realized by coupling the opposite WTe₂ crystal surfaces.

PACS numbers: 73.40.Qv 71.30.+h

I. INTRODUCTION

Recent renewal of interest to semimetals is mostly connected with topological effects. Weyl semimetals are conductors whose low-energy bulk excitations are Weyl fermions¹. Like other topological materials²⁻⁵, Weyl semimetals are characterized by topologically protected metallic surface states, which are known as Fermi arc surface states. This concept of the Fermi arc surface states has now been extended to type II materials¹, like MoTe₂ and WTe₂, which contain electron and hole pockets^{6,7}. The non-trivial properties of these materials have been demonstrated in magnetotransport experiments^{8,9}.

Topological materials exhibit non-trivial physics in proximity with a superconductor¹⁰⁻¹². For the topological insulators¹³⁻¹⁵, it is expected to allow topological superconductivity regime^{16,17}, which stimulates a search for Majorana fermions¹⁸. In the case of Weyl semimetals, the proximity is predicted¹⁹ to produce specular Andreev reflection^{20,21}, or even to superconducting correlations within a semimetal²²⁻²⁴. Moreover, topological transport is responsible for Josephson current in 1-2 μm long superconductor-normal-superconductor (SNS) junctions in graphene^{25,26}.

The edge current contribution can be retrieved even for systems with conducting bulk by analyzing Josephson current suppression in low magnetic fields^{17,28}. The maximum supercurrent is periodically modulated, with period which is defined by the magnetic flux quantum $\Phi_0 = \pi\hbar c/e$. It is well known, that the homogeneous supercurrent density in the conductor corresponds to a single-slit Fraunhofer pattern²⁹. As the edge currents emerge in a two-dimensional topological system, the sinusoidal oscillation pattern appears^{17,28}, which is a fingerprint of a superconducting quantum interference device (SQUID)²⁹. It is therefore reasonable to study Josephson current suppression in a long SNS junction on a three-dimensional Weyl semimetal surface.

Here, we experimentally study electron transport between two superconducting indium leads, coupled to the

WTe₂ crystal surface. WTe₂ is characterized by presence of Fermi arc surface states, as a predicted type-II Weyl semimetal candidate. We demonstrate Josephson current in unprecedentedly long 5 μm In-WTe₂-In junctions, which is confirmed by $I - V$ curves evolution with temperature and magnetic field. The Josephson current is mostly carried by the topological surface states, which we demonstrate in a double-slit SQUID geometry, realized by coupling the opposite WTe₂ crystal surfaces.

II. SAMPLES AND TECHNIQUE

WTe₂ compound was synthesized from elements by reaction of metal with tellurium vapor in the sealed silica ampule. The WTe₂ crystals were grown by the two-stage iodine transport³⁰, that previously was successfully applied^{30,31} for growth of other metal chalcogenides like NbS₂ and CrNb₃S₆. The WTe₂ composition is verified by energy-dispersive X-ray spectroscopy. The X-ray diffraction (Oxford diffraction Gemini-A, MoK α) confirms $Pmn21$ orthorhombic single crystal WTe₂ with lattice parameters $a = 3.48750(10)$ \AA , $b = 6.2672(2)$ \AA , and $c = 14.0629(6)$ \AA . We check by standard magnetoresistance measurements that our WTe₂ crystals demonstrate large, non-saturating positive magnetoresistance up to 14 T field, as it has been shown for WTe₂ Weyl semimetal⁸.

A sample sketch is presented in Fig. 1. Superconducting leads are formed by lift-off technique after thermal evaporation of 100 nm indium on the insulating SiO₂ substrate. A WTe₂ single crystal ($\approx 0.5\text{mm} \times 100\mu\text{m} \times 0.5\mu\text{m}$ dimensions) is weakly pressed to the indium leads pattern, so that planar In-WTe₂ junctions ($10 \times (\approx 5)\mu\text{m}^2$) are formed at the bottom surface of the crystal WTe₂ in Fig. 1.

Charge transport is investigated between two superconducting indium leads in a four-point technique. An example of electrical connections is presented in Fig. 1 : the S1 electrode is grounded; a current I is fed through the S2; a voltage drop V is measured between these S1

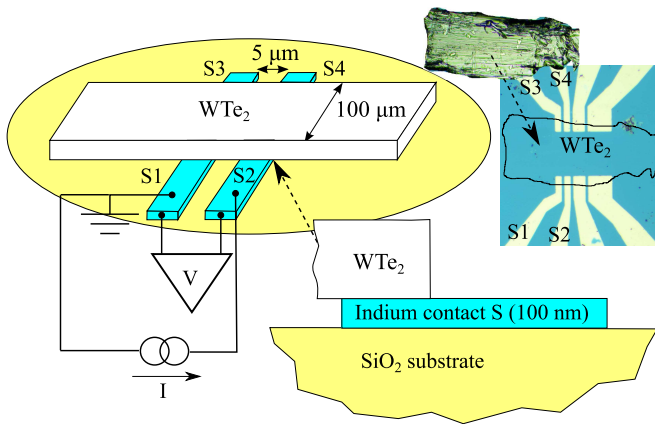


FIG. 1. (Color online) Sketch of the sample with indium contacts to the bottom surface of a WTe_2 crystal (not to scale). Right inset demonstrates top-view images of the indium leads and WTe_2 crystal. $10\ \mu\text{m}$ wide indium superconducting leads (S1-S4) are formed on the insulating SiO_2 substrate. $5\ \mu\text{m}$ long In- WTe_2 -In junctions are fabricated by weak pressing a WTe_2 crystal ($\approx 0.5\text{mm} \times 100\ \mu\text{m} \times 0.5\ \mu\text{m}$) to the indium leads pattern. Charge transport is investigated between two superconducting electrodes in a four-point technique: the S1 electrode is grounded; a current I is fed through the S2; a voltage drop V is measured between these S1 and S2 electrodes by independent wires because of low normal In- WTe_2 -In resistance.

and S2 electrodes by independent wires. In this connection scheme, all the wire resistances are excluded, which is necessary for low-impedance In- WTe_2 -In junctions (below $0.5\ \text{Ohm}$ normal resistance in the present experiment). The measurements are performed in standard He^4 cryostat in the temperature range $1.4\ \text{K} - 4.2\ \text{K}$. The indium leads are superconducting below the critical temperature³² $T_c \approx 3.4\ \text{K}$.

III. EXPERIMENTAL RESULTS

To obtain $I-V$ characteristics, we sweep the dc current I and measure the voltage drop V . Fig. 2 presents $I-V$ examples in two different experimental configurations.

In zero magnetic field, at low temperature $1.4\ \text{K} < T_c$, transport between two $5\ \mu\text{m}$ spaced contacts S1 and S2 is of clear Josephson-like behavior²⁹, as shown by the blue curve in Fig. 2: (i) by the four-point connection scheme we directly demonstrate zero resistance region at low currents; (ii) the non-zero resistance appears as sharp jumps at current values $\pm I_c \approx 4\ \text{mA}$. The jump positions are subjected to small hysteresis with the sweep direction, so they are slightly different for two $I-V$ branches in Fig. 2. Because of similar preparation technique, different samples demonstrate even quantitatively similar behavior: the obtained I_c values differ within 10% of magnitude for different samples and in different coolings. In contrast, the resistance is always finite between $80\ \mu\text{m}$ separated S1 and S3 indium leads, see the red curve in

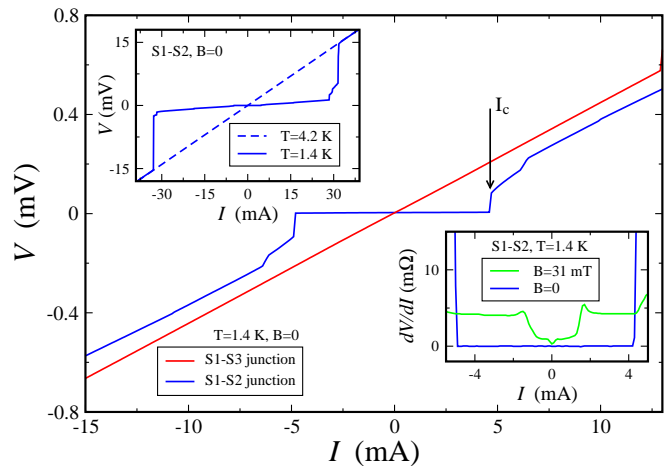


FIG. 2. (Color online) Examples of $I-V$ characteristics in two different experimental configurations in zero magnetic field at $1.4\ \text{K} < T_c$. The blue curve is obtained for $5\ \mu\text{m}$ long In- WTe_2 -In junction between the superconducting leads S1 and S2, as depicted in Fig. 1. A clear Josephson behavior can be seen: there is no resistance at low currents, it appears above $\pm I_c \approx 4\ \text{mA}$. In contrast, the resistance is always finite between $80\ \mu\text{m}$ separated S1 and S3 indium leads, see the red curve. Left inset: superconductivity suppression in indium leads S1 and S2 by current $\approx \pm 30\ \text{mA}$ (the solid curve, $T = 1.4\ \text{K}$) or temperature (the dashed one, $T = 4.2\ \text{K} > T_c$) in zero magnetic field. Right inset: $dV/dI(I)$ characteristics for the S1- WTe_2 -S2 junction at minimal $T = 1.4\ \text{K}$, obtained in zero field (the blue curve) and for the critical $B_c = 31\ \text{mT}$ (the green one).

Fig. 2.

Even for the closely-spaced contacts S1 and S2, $I-V$ curve can be switched to standard Ohmic behavior, if the indium superconductivity is suppressed by temperature or high current (above $\approx 30\ \text{mA}$ for the present dimensions), as depicted in the left inset to Fig. 2. The zero-resistance state can also be suppressed by magnetic field, as it is demonstrated in the right inset to Fig. 2.

Thus, we demonstrate in Fig. 2, that two superconducting contacts induce Josephson current in an unprecedentedly long $5\ \mu\text{m} \gg \xi_{In}$ In- WTe_2 -In junction, where $\xi_{In} \approx 300\ \text{nm}$ is the indium correlation length³².

As usual for SNS junctions, an important information can be obtained from the maximum supercurrent I_c suppression by temperature and magnetic field. To analyze $I_c(B, T)$ behavior, we use $dV/dI(I)$ characteristics like ones presented in the right inset to Fig. 2: the dc current is additionally modulated by a low ac component ($100\ \text{nA}$, $10\ \text{kHz}$), an ac part of V ($\sim dV/dI$) is detected by a lock-in amplifier. We have checked, that the lock-in signal is independent of the modulation frequency in the $6\ \text{kHz} - 30\ \text{kHz}$ range, which is defined by applied ac filters. To obtain I_c values with high accuracy for given (B, T) values, we sweep current I ten times from zero (superconducting state) to above I_c (resistive state), and then determine I_c as the average value of dV/dI jump

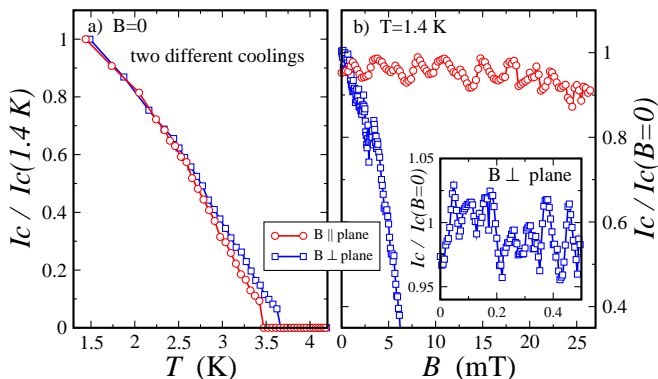


FIG. 3. (Color online) Suppression of the maximum supercurrent I_c by temperature (a) or magnetic field (b). (a) $I_c(T)$ monotonously falls to zero at 3.5 K, which well corresponds to the indium critical temperature (different symbols refer to different sample coolings). The curves are obtained in zero magnetic field. (b) $I_c(B)$ suppression pattern crucially depends on the magnetic field orientation to the In-WTe₂-In junction plane: it is extremely strong for the perpendicular field, while it is very slow (within 10% until the critical field) for the parallel orientation. For both orientations, there are oscillations in $I_c(B)$, the period is much higher for the parallel magnetic field (2 mT and 0.1 mT, respectively). The curves are obtained at minimal 1.4 K temperature.

positions in different sweeps.

The results are presented in Fig. 3. $I_c(T)$ monotonously falls to zero at 3.5 K, which well corresponds to the indium critical temperature³², see Fig. 3 (a). However, $I_c(T)$ does not demonstrate the exponential decay, which is expected³⁴ for long $L \gg \xi_{In}$ SNS junctions. Instead, the experimental $I_c(T)$ dependence is even slower than the linear function of T in Fig. 3 (a), as it is usually realized for the short $L < \xi_{In}$ junction regime³⁴.

To our surprise, $I_c(B)$ suppression pattern crucially depends on the magnetic field orientation to the In-WTe₂-In junction plane, see Fig. 3 (b). If the magnetic field is perpendicular to the plane, strong suppression of $I_c(B)$ is observed, which is usual for standard Josephson effect²⁹. In contrast, $I_c(B)$ is diminishing very slowly (within 10% until the indium critical field) for the parallel magnetic field. For both orientations, we observe equidistant $I_c(B)$ oscillations within 5% of I_c magnitude, see also inset to Fig. 3 (b). The oscillations are characterized by high $\Delta B = 2$ mT period for the parallel field and by low $\Delta B = 0.1$ mT for the perpendicular one. It can be easily seen, that the observed $I_c(B)$ suppression in parallel magnetic fields resembles double-slit SQUID behavior^{17,28}, so the surface transport is important in WTe₂.

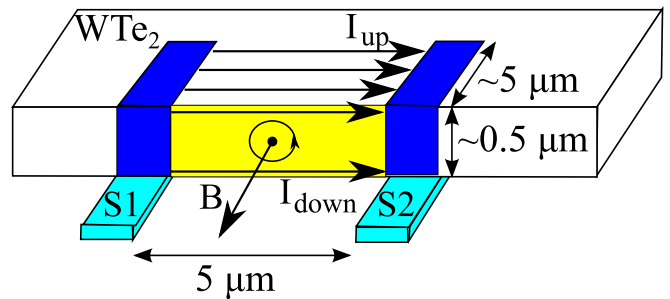


FIG. 4. (Color online) Schematic diagram of a double-slit SQUID geometry, realized by Weyl surface states in WTe₂ semimetal. Superconductivity is proximity induced near the In leads (blue regions) between the opposite sample surfaces, since $d \sim \xi$. Josephson current (denoted by arrows) is transferred by top and bottom surface states simultaneously. Thus, there are two parallel SNS junctions, which form a double-slit SQUID geometry. The effective SQUID area is denoted by yellow (see the main text for details).

IV. DISCUSSION

The experimental $I_c(T, B)$ dependencies allows us to unambiguously identify the topological effects.

Slow $I_c(T)$ decay has been reported in long $1.5-2 \mu\text{m} \gg \xi$ SNS junctions on graphene, and has been connected with topological transport^{25,26}. WTe₂ is regarded as type-II Weyl semimetal⁷⁻⁹, which contains topological Fermi arc surface states. These surface states are usually decoupled from the bulk^{35,36}. On the other hand, Weyl surface states inherit the chiral property of the Chern insulator edge states¹. Because of topological protection, they can efficiently transfer the Josephson current. This might be a reason^{25,26} to have slow $I_c(T)$ dependence³³ in our nominally long $\gg \xi_{In} \approx 300$ nm devices.

We should connect $I_c(B)$ behavior with the distribution of the Josephson current within the WTe₂ crystal, see Fig. 4. The sample thickness is comparable with indium coherence length $\sim \xi_{In} \approx 300$ nm, so the regions of proximity-induced superconductivity couples two opposite sample surfaces near the In leads (blue regions in Fig. 4). The Josephson current is transferred by topological surface states, so there are two parallel weak links between the superconducting leads. In other words, a non-symmetric double-slit SQUID geometry^{17,28} is realized, see Fig. 4.

The experimental $I_c(B)$ suppression pattern well corresponds to the double-slit SQUID^{17,28} with two non-equivalent weak links. Parallel magnetic field induces a phase shift between the opposite WTe₂ surfaces, so it controls the magnetic flux through the effective SQUID area, see Fig. 4. The latter can be estimated ($S\Delta B \sim \Phi_0$) from $\Delta B = 2$ mT as $S \approx 10^{-8} \text{cm}^2$, which gives $0.3 \mu\text{m}$ sample thickness for our $5 \mu\text{m}$ long junctions. This estimation is in good correspondence with the known WTe₂ crystal thickness.

If the magnetic field is perpendicular to the WTe₂ crys-

tal plane, there is no phase shift between the the opposite sample surfaces. Instead, $I_c(B)$ reflects homogeneous supercurrent distribution within the surface state in two equivalent SNS junctions. Thus, we observe strong $I_c(B)$ suppression in Fig. 3 (b) with oscillations in low fields²⁹, which reflects the effective junction area S . The experimentally observed period $\Delta B = 0.1$ mT in the inset to Fig. 3 (b) corresponds to $S \approx 2 \times 10^{-7} \text{cm}^2$, i.e. to the $\approx 5 \mu\text{m} \times 5 \mu\text{m}$ SNS junctions, which well correspond to the sample dimensions.

V. CONCLUSION

As a conclusion, we experimentally study electron transport between two superconducting indium leads, coupled to the WTe₂ crystal surface. WTe₂ is charac-

terized by presence of Fermi arc surface states, as a predicted type-II Weyl semimetal candidate. We demonstrate Josephson current in unprecedentedly long $5 \mu\text{m}$ In-WTe₂-In junctions, which is confirmed by $I-V$ curves evolution with temperature and magnetic field. The Josephson current is mostly carried by the topological surface states, which we demonstrate in a double-slit SQUID geometry, realized by coupling the opposite WTe₂ crystal surfaces.

ACKNOWLEDGMENTS

We wish to thank Ya. Fominov, V.T. Dolgoplov, V.A. Volkov for fruitful discussions, and S.S Khasanov for X-ray sample characterization. We gratefully acknowledge financial support by the RFBR (project No. 16-02-00405) and RAS.

-
- ¹ As a recent review see N. P. Armitage, E. J. Mele, and Ashvin Vishwanath, *Reviews of Modern Physics* (2017), arXiv:1705.01111
- ² M. Z. Hasan and C. L. Kane, *Rev. Mod. Phys.* 82, 3045 (2010).
- ³ X.-L. Qi and S.-C. Zhang, *Rev. Mod. Phys.* 83, 1057 (2011).
- ⁴ A. Bansil, H. Lin, and T. Das, *Rev. Mod. Phys.* 88, 021004 (2016).
- ⁵ C.-K. Chiu, J. C. Teo, A. P. Schnyder, and S. Ryu, *Rev. Mod. Phys.* 88, 035005 (2016).
- ⁶ Deng K., Wan G., Deng P., Zhang K., Ding S., Wang E., Yan M., Huang H., Zhang H., Xu Z., Denlinger J., Fedorov A., Yang H., Duan W., Yao H., Wu Y., Fan S., Zhang H., Chen X., Zhou S., *Nat. Phys.* 12, 11051110 (2016).
- ⁷ Chenlu Wang et al., *Phys. Rev. B* 94, 241119(R)
- ⁸ Mazhar N. Ali, Jun Xiong, Steven Flynn, Jing Tao, Quinn D. Gibson, Leslie M. Schoop, Tian Liang, Neel Hal-dolaarachige, Max Hirschberger, N. P. Ong and R. J. Cava *Nature* 514, 205 (2014). doi:10.1038/nature13763
- ⁹ Wang, Y. et al., *Nat. Commun.* 7, 13142 (2016). doi: 10.1038/ncomms13142
- ¹⁰ A. Kononov, V.A. Kostarev, B.R. Semyagin, V.V. Pre-obrazhenskii, M.A. Putyato, E.A. Emelyanov, and E.V. Deviatov, *Physical Review B* 96, 245304 (2017). DOI: 10.1103/PhysRevB.96.245304
- ¹¹ A. Kononov, S. V. Egorov, Z. D. Kvon, N. N. Mikhailov, S. A. Dvoretzky, and E. V. Deviatov, *Phys. Rev. B* 93, 041303(R) (2016)
- ¹² A. Kononov, S. V. Egorov, N. Titova, Z. D. Kvon, N. N. Mikhailov, S. A. Dvoretzky, E. V. Deviatov, *JETP Lett.*, 101, 41 (2015).
- ¹³ S. Murakami, N. Nagaosa, S.-C. Zhang, *Phys. Rev. Lett.* 93, 156804 (2004).
- ¹⁴ C. L. Kane, E. J. Mele, *Phys. Rev. Lett.* 95, 146802 (2005).
- ¹⁵ B. A. Bernevig, S.-C. Zhang, *Phys. Rev. Lett.* 96, 106802 (2006).
- ¹⁶ L. Fu and C. L. Kane, *Phys. Rev. Lett.* 100, 96407 (2008).
- ¹⁷ S. Hart, H. Ren, T. Wagner, Ph. Leubner, M. Mühlbauer, C. Brüne, H. Buhmann, L. W. Molenkamp and A. Yacoby, *Nature Physics* 10, 638643 (2014).
- ¹⁸ For recent reviews, see C. W. J. Beenakker, *Annu. Rev. Con. Mat. Phys.* 4, 113 (2013) and J. Alicea, *Rep. Prog. Phys.* 75, 076501 (2012).
- ¹⁹ Wei Chen, Liang Jiang, R. Shen, L. Sheng, B. G. Wang, D. Y. Xing *EPL* 103, 27006 (2013)
- ²⁰ C. W. J. Beenakker, *Physical Review Letters* 97 (2006).
- ²¹ C. W. J. Beenakker, *Reviews of Modern Physics* 80, 1337 (2008).
- ²² T. Meng and L. Balents, *Phys. Rev. B* 86, 054504 (2012).
- ²³ G. Y. Cho, J. H. Bardarson, Y.-M. Lu, and J. E. Moore, *Phys. Rev. B* 86, 214514 (2012).
- ²⁴ H. Wei, S. P. Chao, and V. Aji, *Phys. Rev. B* 89, 014506 (2014).
- ²⁵ V. E. Calado, S. Goswami, G. Nanda, M. Diez, A. R. Akhmerov, K. Watanabe, T. Taniguchi, T. M. Klapwijk & L. M. K. Vandersypen, *Nature Nanotechnology* 10, 761764 (2015). doi:10.1038/nnano.2015.156
- ²⁶ I.V. Borzenets, F. Amet, C.T. Ke, A.W. Drae-los, M.T. Wei, A. Seredinski, K. Watanabe, T. Taniguchi, Y. Bomze, M. Yamamoto, S. Tarucha, and G. Finkelstein, *Phys. Rev. Lett.* 117, 237002 (2016), <http://dx.doi.org/10.1103/PhysRevLett.117.237002>
- ²⁷ Sean Hart, Hechen Ren, Timo Wagner, Philipp Leubner, Mathias Mühlbauer, Christoph Brne, Hartmut Buhmann, Laurens W. Molenkamp & Amir Yacoby, *Nature Physics* 10, 638643 (2014), doi:10.1038/nphys3036
- ²⁸ Vlad S. Pribiag, Arjan J. A. Beukman, Fanming Qu, Maja C. Cassidy, Christophe Charpentier, Werner Wegscheider & Leo P. Kouwenhoven, *Nature Nanotechnology* 10, 593 (2015)
- ²⁹ M. Tinkham, *Introduction to Superconductivity* (2d ed., McGrawHill, New York, 1996).
- ³⁰ E. B. Borisenko, V. A. Berezin, N. N. Kolesnikov, V. K. Gartman, D. V. Matveev, O. F. Shakhlevich, *Physics of the Solid State*, 59, 1310, (2017).
- ³¹ A. Sidorov, A.E. Petrova, A.N. Pinyagin, N.N. Kolesnikov, S.S. Khasanov, S.M. Stishov, *JETP*, 122, 1047, (2016).
- ³² A. M. Toxen *Phys. Rev.* 123, 442 (1961).

- ³³ I.O. Kulik and A.N. Omelyanchuk, *Fiz. Nizk. Temp.* 3, 945 (1977) [*Sov. J. Low Temp. Phys.* 3, 459 (1977)].
- ³⁴ I. O. Kulik, *Sov. Phys. JETP* 30, 944 (1970).
- ³⁵ Marco Bianchi, Richard C. Hatch, Jianli Mi, Bo Brummerstedt Iversen, and Philip Hofmann, *Phys. Rev. Lett.* 107, 086802 (2011)
- ³⁶ O.O. Shvetsov, V.A. Kostarev, A. Kononov, V.A. Golyashov, K.A. Kokh, O.E. Tereshchenko, and E.V. Deviatov, *EPL* 119, 57009 (2017), doi:10.1209/0295-5075/119/57009